*Jelena Lađarević[1], Bojan Božić[2], Dušan Mijin[1], Luka Matović[3], Nataša Valentić[1], Evica Ivanović[4], Nebojša Banjac[4]**

[1]Faculty of Technology and Metallurgy, University of Belgrade, Belgrade, Serbia, [2]Institute of Physiology and Biochemistry "Ivan Djaja", Faculty of Biology, University of Belgrade, Belgrade, Serbia, [3]Innovation Centre of the Faculty of Technology and Metallurgy, University of Belgrade, Belgrade, Serbia, [4]Faculty of Agriculture, University of Belgrade, Belgrade, Serbia

Scientific paper
ISSN 0351-9465, E-ISSN 2466-2585
https://doi.org/10.62638/ZasMat1394

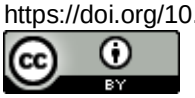

Zastita Materijala 67 (1)
119 - 132 (2026)

Study of tautomerism and solvatochromism of 5-(substituted phenylazo)-3-cyano-6-hydroxy-4-methyl-2-pyridones

ABSTRACT

In this study, ten 5-(substituted phenylazo)-3-cyano-6-hydroxy-4-methyl-2-pyridone dyes were synthesized, differing in both the position and the nature of substituents on the phenyl ring. The structural characterization of the dyes was performed using melting point analysis, FT-IR, NMR, and UV-Vis spectroscopy. The study includes spectral determination of the possible tautomeric forms in both the solid state and various solvents. Solvatochromic properties are investigated in 21 solvents with varying properties to assess the impact of solvent-solute interactions and effects of substituents electronic nature on the absorption maxima. For quantitative evaluation of the non-specific and specific solvent effects on the UV-Vis absorption maxima, the principles of the linear solvation energy relationships are used, i.e. models proposed by Kamlet-Taft and Catalán. Based on electronic distribution and substituent effects, methoxy-substituted dyes in ortho- and para-positions of phenyl ring have emerged as the most promising candidates for corrosion inhibition.
Keywords: *pyridone azo dyes, tautomerism, hydrazone, LSER*

1. INTRODUCTION

Azo dyes, as synthetic compounds, are extensively utilized in food, pharmaceutical, cosmetic, and textile industries, characterized by their structurally diverse molecules [1,2]. Additionally, it should be noted that azo dyes account for over 60% of the total production of all types of dyes, while approximately 70% make up the share of applied dyes in the industry [3].

Pyridone azo dyes are easy to synthesize and have good stability, whereby their structure consists of a pyridone ring, coupled with a heterocyclic or carbocyclic ring. Pyridone azo dyes have different applications. Alongside their usage as dyeing textiles, they are used in LCD screens, as liquid crystals, and in inkjet printing as pigments [4-7].

The use of organic compounds as corrosion inhibitors is commonly employed to extend the lifecycle of metals. These inhibitors form a protective barrier by adsorption onto the metal surface, shielding it from the harmful environment.

∗Corresponding author: Nebojša Banjac
E-mail: nbanjac@agrif.bg.ac.rs
Paper received: 06.03. 2025.
Paper corrected: 28.05. 2025.
Paper accepted: 02. 06.2025.

The adsorption is facilitated by their active centers, which include polar functional groups, heteroatoms (such as N, S, O, P), aromatic rings, and π-electrons [8]. Corrosion prevention commonly involves the use of various heterocyclic organic compounds, particularly those belonging to the pyridine, imidazole, quinoline and azole groups [9]. On the other hand, the polar functional groups like hydroxyl, nitro, azo, carboxylic, cyano, carbonyl, imine, also, act as adsorption centers [10]. The ability of a particular organic compound to inhibit metal corrosion is influenced by two factors: the electronic distribution and the chemical structure [11].

Azo dyes function as corrosion inhibitors in various mixtures of electrolytes and metals and are one of the most commonly used anti-corrosion materials [12, 13, 14,15] due to their molecular structures, which contain numerous donor sites that allow them to act as chelating ligands when interacting with metal surfaces [12,16]. Non-bonding electrons from the nitrogen atom as well as the π-orbitals of the azo group (–N=N–) can participate in electron donation [13, 17,18]. Moreover, the empty p-orbitals of the nitrogen atoms can participate in the acceptance of electrons from the metal d-orbitals (retro donation)

[17]. Studies suggest that the nature of substituents can significantly affect their corrosion inhibition efficiency, with electron-donating groups, particularly in the *para*-position to azo bridge, often enhance performance by increasing electron density and promoting stronger interactions with metal surfaces [14,15,18].

In our previous study [19], we demonstrated that azo pyridone dyes act as effective chelating agents, as evidenced by the successful synthesis of two Cu(II) complexes. Having this in mind, the present study reports synthesis of ten 5-(substituted phenylazo)-3-cyano-6-hydroxy-4--methyl-2-pyridones altering both the position (*-ortho*, *-meta* and *-para*) and the nature (–OMe, $–NO_2$ and –Cl) of substituents in the phenyl group(Fig.1). The structures of the synthesized compounds are confirmed by FT-IR, ^{1}H NMR, ^{13}C NMR and UV-Vis spectroscopy and elemental analysis for compounds **2** and **6**. Literature data on similar azo pyridone dyes [20,21] suggest that these dyes exhibit azo-hydrazone tautomerism, due to the presence of the –OH group conjugated with the azo bridge (Fig. 1). Notably, most studies on the corrosion inhibition of azo dyes neglect this phenomenon, despite its critical importance for understanding the structure-property relationship since the migration of the proton within the molecule leads to a change in the structural skeleton, electron density distribution and physicochemical properties. Therefore, the primary aim of this study is to identify the dominant tautomeric form of the synthesized dyes in both the solid state and in various solvents by different spectroscopic techniques. The effects of the electronic nature of the substituents on the position of UV-Vis spectra are assessed. The nature of solvent-solute interactions plays a key role in stabilizing a particular tautomer, affecting electron distribution at different functional groups and molecular geometry [22]. To quantify these effects, the influence of both non-specific and specific solvent-solute interactions on the UV-Vis absorption maxima was evaluated using the LSER (Linear Solvation Energy Relationship) approach. The resulting solvatochromic data were analyzed using Kamlet-Taft and Catalán equations. As such, this study offers a theoretical framework focused on the structural and molecular characteristics of azo dyes that affect their potentialas corrosion inhibitors, providing a pathway for the design of more efficient corrosion-resistant materials.

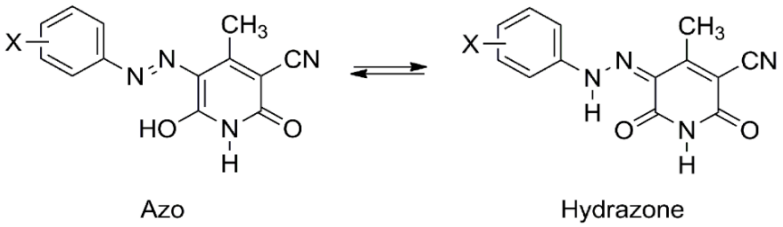

Copmounds	X
1	4-OCH_3
2	3-OCH_3
3	2-OCH_3
4	4-NO_2
5	3-NO_2
6	2-NO_2
7	4-Cl
8	3-Cl
9	2-Cl
10	H

*Figure 1. Azo-hydrazone tautomerism of the investigated dyes **1–10***

2. EXPERIMENTAL

2.1. Materials and measurements for the compounds

The reagents used for the synthesis were purchased from Merck, Sigma Aldrich and Fluka, and were used without purification. Additionally, solvents of spectroscopic purity were taken from the same manufacturers. Microwave-assisted syntheses were carried out using a household microwave oven Samsung M182 DN. The structure of the synthesized molecules was confirmed by determining the melting point, FT-IR, ^{1}H NMR, ^{13}C NMR and elemental analysis.The melting point of the synthesized compounds was determined by using the melting point system Stuart SMP30. ^{1}H NMR, ^{13}C NMR spectra of the compounds were recorded using a Varian Gemini 2000 (400 Hz and 100 Hz respectively) in deuterated DMSO-d_6 and CF_3COOD with TMS as an internal standard. The FTIR spectra of the synthesized compounds were determined using a Nicolet™ iS™ 10 FT-IR Spectrometer (Thermo Fisher SCIENTIFIC) with Smart iTR™ Attenuated Total Reflectance (ATR) Sampling accessories in the range of 500–4000 cm^{-1}, with 32 scans per spectrum. Elemental analysis was performed on a Vario EL III elemental analyzer. UV-Vis absorption spectra of the synthesized dyes were determined by using a Shimadzu 1700 spectrophotometer. The concentrations of all tested compounds in solvents were 5×10^{-5} M.

2.2. Synthesis of arylazo pyridone dyes

The synthesis of arylazo pyridone dyes was carried out in two steps. The first step involved the microwave synthesis of the starting 3-cyano-6-hydroxy-4-methyl-2-pyridone (Fig. 2) [23], which was carried out according to the following procedure. Ethyl-acetoacetate (0.02 mol, 2.6 g), cyanoacetamide (0.02 mol, 1.68 g) and powdered potassium hydroxide (0.02 mol, 1.12 g) were mixed in a test tube and heated in a commercial microwave oven at 200 W by irradiation for 4 minutes.

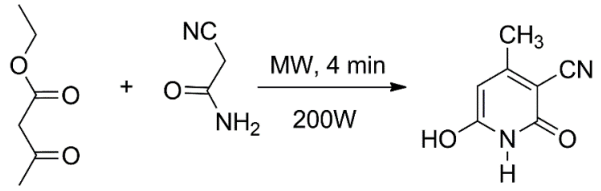

Figure 2. Microwave synthesis of 3-cyano-6--hydroxy-4-methyl-2-pyridone

The resulting reaction mixture was treated three times with 10 mL of H_2O under gentle heating until the precipitate completely dissolved. After cooling, the solution was filtered, and the filtrate was then acidified with HCl, whereby a white precipitate was separated. The product was separated by filtration, washed twice with water (5 mL) and air-dried. A white substance was obtained, with a yield of 60%; m.p. 315–316 °C (lit. m.p. 315–320 °C [24]), FT-IR (KBr, v/cm^{-1}): 3294 (OH), 2223 (CN), 1593 (C=O); ^{1}H NMR (200 MHz, DMSO-d_6, δ/ppm): 2.51 (3H, s, CH_3), 5.61 (1H, s, C_5).

The second step in the synthesis of the dyes represents a classical diazo-coupling reaction (Fig. 3). Substituted aniline derivatives (10 mmol) were dissolved in concentrated hydrochloric acid (2.5 mL) and cooled to –5 °C. Sodium nitrite (1.23 g, 11 mmol) was dissolved in cold water (4 mL) and added in drops to the aniline solution. The mixture was stirred for 1 h to give the diazonium salt of the corresponding aniline. The obtained pyridone (10 mmol) was dissolved in an aqueous solution (4 mL) of potassium hydroxide (0.56 g, 10 mmol) and cooled to –5 °C. The diazonium salt was added dropwise to the pyridone solution, which was stirred for half an hour. The mixture was then stirred for an additional 3 hours, while the temperature was maintained between 0 and 5 °C. Once the mixture had been refrigerated overnight, it was filtrated, rinsed with water, and dried. The compounds **1**–**3** were recrystallized from chloroform, while the rest of the compounds were recrystallized from *N*,*N*-dimethylformamide (DMF). It should be noted that eight compounds are already known and registered in the literature, while compound **6** is present in the patent literature, and compound **2** is a new molecule.

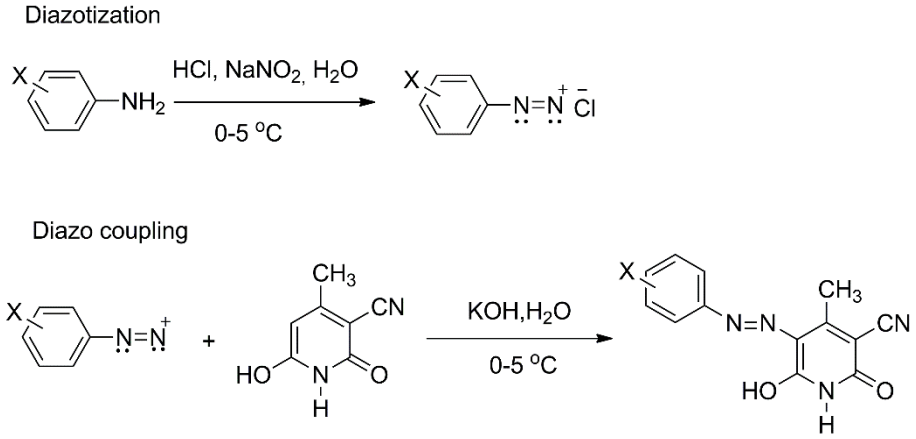

*Figure 3. Synthesis of compounds **1–10***

5-(4-Methoxyphenylazo)-3-cyano-6-hydroxy-4--methyl-2-pyridone (**1**). Dark red powder, yield: 59%, m.p. 270.3–271.1 °C (lit. m.p. 272–273 °C [25,26], 270–271 °C [27]); M = 284.3 g mol^{-1}; FT-IR (KBr, v/cm^{-1}): 3433 (NH hydrazone form), 3121 (NH pyridone), 2221 (CN), 1675, 1630 (C=O pyridone); ^{1}H NMR (200 MHz, DMSO-d_6, δ/ppm): 2.50 (3H, s, CH_3), 3.80 (3H, s, OCH_3), 7.06 (2H, d, *J* = 8.4 Hz, Ar–H), 7.65 (2H, d, *J* = 8.4 Hz, Ar–H), 11.96 (1H, s, NH pyridone), 14.78 (1H, s, NH hydrazone form); ^{13}C NMR (50 MHz, DMSO-d_6, δ/ppm): 161.7 (Py), 161.1 (Py), 160.5 (Py), 158.8 (Ar), 134.7 (Ar), 122.8 (Py), 119.2 (Ar), 115.5 (CN), 115.3 (Ar), 99.5 (Py), 55.7 (OCH_3), 16.6 (CH_3); UV-Vis (EtOH) (λ_{max}/nm (log ε)): 457 (3.99).

5-(3-Methoxyphenylazo)-3-cyano-6-hydroxy-4--methyl-2-pyridone (**2**). Dark red powder; yield: 33%; m.p. 287.3–288.1 °C; M = 284.3 g mol^{-1}; Calculated $C_{14}H_{12}N_4O_3$ (%): C, 59.15; H, 4.25; N, 19.71; Found (%): C, 59.05; H, 4.29 ; N,19.68; FT-IR (KBr, v/cm^{-1}): 3436 (NH hydrazone form), 3137 (NH pyridone), 2226 (CN), 1668, 1649 (C=O

pyridone); ^{1}H NMR (200 MHz, DMSO-d_6, δ/ppm): 2.50 (3H, s, CH_3), 3.80 (3H, s, OCH_3), 6.81 (1H, d, *J* = 8.4 Hz, Ar–H), 7.18–7.20 (2H, m, Ar–H), 7.34 (1H, t, *J* = 8.2 Hz, Ar–H), 12.01 (1H, s, NH pyridone), 14.44 (1H, s, NH hydrazone form); ^{13}C NMR (50 MHz, DMSO-d_6, δ/ppm): 161.7 (Py), 161.0 (Py), 160.7 (Py), 160.6 (Ar), 142.5 (Ar), 131.0 (Ar), 123.8 (Py), 115.2 (CN), 112.8 (Ar), 109.7 (Ar), 102.8 (Ar), 101.1 (Py), 55.6 (OCH_3), 16.7 (CH_3); UV-Vis (EtOH) (λ_{max}/nm (log ε)): 435.6 (4.51).

5-(2-Methoxyphenylazo)-3-cyano-6-hydroxy-4--methyl-2-pyridone (**3**). Red powder; yield: 61%; m.p. 317.1–318.5 °C (lit. m.p. 324–325 °C [25], 314–315 °C [27]); M = 284.3 g mol^{-1}; FT-IR (KBr, v/cm^{-1}): 3436 (NH hydrazone form), 3143 (NH pyridone), 2221 (CN), 1669, 1650 (C=O pyridone); ^{1}H NMR (200 MHz, DMSO-d_6, δ/ppm): 2.50 (3H, s, CH_3), 3.92 (3H, s, OCH_3), 7.00–7.33 (2H, m, Ar–H), 7.61 (1H, d, *J* = 7.2 Hz, Ar–H), 7.75 (1H, d, *J* = 7.4 Hz, Ar–H), 12.06 (1H, s, NH pyridone), 14.91 (1H, s, NH hydrazone form); ^{13}C NMR (50 MHz, DMSO-d_6, δ/ppm): 161.4 (Py), 160.9 (Py), 160.0 (Py), 149.0 (Ar), 142.3 (Ar), 131.0 (Ar), 128.2 (Ar), 122.1 (Py), 121.5 (Ar), 115.7 (CN), 112.6 (Ar), 101.0 (Py), 56.6 (OCH_3), 16.6 (CH_3); UV-Vis (EtOH) (λ_{max}/nm (log ε)): 453.0 (4.01).

5-(4-nitrophenylazo)-3-cyano-6-hydroxy-4--methyl-2-pyridone (**4**). Dark orange powder; yield: 54%; m.p. 326.2–327.8 °C (lit. m.p. 326–327 °C [25,26], 324 °C [28], 326–328 °C [29], > 320 °C [30]); M = 299.2 g mol^{-1}; FT-IR (KBr, v/cm^{-1}): 3446 (NH hydrazone form), 3110 (NH pyridone), 2229 (CN), 1680, 1638 (C=O pyridone); ^{1}H NMR (200 MHz, CF_3COOD, δ/ppm): 2.89 (3H, s, CH_3), 7.92 (2H, d, *J* = 9.0 Hz, Ar–H), 8.53 (2H, d, *J* = 9.0 Hz, Ar–H), 8.56 (1H, s, Ar–H), 11.4 (1H, s, NH pyridone), 14.87 (1H, s, NH hydrazone form); ^{13}C NMR (50 MHz, CF_3COOD, δ/ppm): 163.9 (Py), 162.4 (Py), 161.5 (Py), 147.2 (Ar), 146.5 (Ar), 126.8 (Py), 123.8 (CN), 118.1 (Ar), 112.5 (Ar), 106.9 (Py), 16.7 (CH_3); UV-Vis (EtOH) (λ_{max}/nm (log ε)): 432 (4.36).

5-(3-nitrophenylazo)-3-cyano-6-hydroxy-4--methyl-2-pyridone (**5**). Orange-yellow powder; yield: 52 %; m.p. 275.3–276.6 °C (lit. m.p. 279–280 °C [31]); M = 299.2 g mol^{-1}; FT-IR (KBr, v/cm^{-1}): 3447 (NH hydrazone form), 3089 (NH pyridone), 2224 (CN), 1692, 1645 (C=O pyridone); ^{1}H NMR (200 MHz, CF_3COOD, δ/ppm): 2.80 (3H, s, CH_3), 7.74 (1H, t, *J* = 8.0 Hz, Ar–H), 8.01 (1H, d, *J* = 8.0 Hz, Ar–H), 8.26 (1H, d, *J* = 8.0 Hz, Ar–H), 8.56 (1H, s, Ar–H), 11.3 (1H, s, NH pyridone), 14.87 (1H, s, NH hydrazone form); ^{13}C NMR (50 MHz, CF_3COOD, δ/ppm): 163.5 (Py), 162.6 (Py), 161.8 (Py), 150.3 (Ar), 142.8 (Ar), 132.5 (Py), 125.2 (Ar), 124.2 (Ar), 124.1 (CN), 118.5 (Ar), 112.9 (Ar), 107.2 (Py), 17.0 (CH_3); UV-Vis (EtOH) (λ_{max}/nm (log ε)): 415.5 (4.16).

5-(2-nitrophenylazo)-3-cyano-6-hydroxy-4--methyl-2-pyridone (**6**). Orange powder; yield: 44%; m.p. 288.5–289.6 °C; M = 299.2 g mol^{-1}; Calculated $C_{13}H_9N_5O_4$ (%): C, 52.18; H, 3.03; N, 23.40; Found (%): C, 52.21; H, 3.09; N, 23.45;FT-IR (KBr, v/cm^{-1}): 3447 (NH hydrazone form), 3157 (NH pyridone), 2227 (CN), 1673, 1654 (C=O pyridone); UV-Vis (EtOH) (λ_{max}/nm (log ε)): 433.5 (3.85).

5-(4-Chlorophenylazo)-3-cyano-6-hydroxy-4--methyl-2-pyridone (**7**). Orange powder; yield: 61%; m.p. 300.2–301.7 °C (lit. m.p. 301–302 °C [25,26], 288–289 °C [29], 302–303 °C [27]); M = 288.7 g mol^{-1}; FT-IR (KBr, v/cm^{-1}): 3446 (NH hydrazone form), 3132 (NH pyridone), 2228 (CN), 1680, 1641 (C=O pyridone); ^{1}H NMR (200 MHz, CF_3COOD, δ/ppm): 2.60 (3H, s, CH_3), 7.31 (2H, d, *J* = 8.0 Hz, Ar–H), 7.43 (2H, d, *J* = 8.0 Hz, Ar–H), 11.4 (1H, s, NH pyridone), 14.84 (1H, s, NH hydrazone form); ^{13}C NMR (50 MHz, CF_3COOD, δ/ppm): 163.8 (Py), 162.9 (Py), 162.1 (Py), 139.8 (Ar), 137.7 (Ar), 131.6 (Py), 124.1 (CN), 118.5 (Ar), 112.9 (Ar), 107.2 (Py), 17.0 (CH_3); UV-Vis (EtOH) (λ_{max}/nm (log ε)): 433.5 (4.39).

5-(3-Chlorophenylazo)-3-cyano-6-hydroxy-4--methyl-2-pyridone (**8**). Orange powder; yield: 33%; m.p. 295.3–296.8 °C (lit. m.p. 288–290 °C [31], 298–300 °C [27]); M = 288.7 g mol^{-1}; FT-IR (KBr, v/cm^{-1}): 3436 (NH hydrazone form), 3105 (NH pyridone), 2227 (CN), 1680, 1636 (C=O pyridone); ^{1}H NMR (200 MHz, CF_3COOD, δ/ppm): 2.81 (3H, s, CH_3), 7.39–7.55 (3H, m, Ar–H), 7.71 (1H, s, Ar–H), 11.3 (1H, s, NH pyridone), 14.91 (1H, s, NH hydrazone form); ^{13}C NMR (50 MHz, CF_3COOD, δ/ppm): 163.8 (Py), 162.8 (Py), 161.9 (Py), 142.3 (Ar), 137.7 (Ar), 132.2 (Py), 130.9 (Ar), 124.1 (CN), 118.7 (Ar), 118.5 (Ar), 112.9 (Ar), 107.2 (Py), 16.9 (CH_3); UV-Vis (EtOH) (λ_{max}/nm (log ε)): 423.5 (4.39).

5-(2-Chlorophenylazo)-3-cyano-6-hydroxy-4--methyl-2-pyridone (**9**). Orange powder; yield: 42%; m.p. 345.6–346.9 °C (lit. m.p. 347–348 °C [25], > 320 °C [27]); M = 288.7 g mol^{-1}; FT-IR (KBr, v/cm^{-1}): 3430 (NH hydrazone form), 3141 (NH pyridone), 2228 (CN), 1670, 1629 (C=Opyridone); ^{1}H NMR (200 MHz, CF_3COOD, δ/ppm): 2.83 (3H, s, CH_3), 7.38–7.57 (3H, m, Ar–H), 7.98 (1H, d, *J* = 7.8 Hz, Ar–H), 11.3 (1H, s, NH pyridone), 15.29 (1H, s, NH hydrazone form); ^{13}C NMR (50 MHz, CF_3COOD, δ/ppm): 163.7 (Py), 162.9 (Py), 162.0 (Py), 137.9 (Ar), 131.5 (Ar), 131.4 (Ar), 129.8 (Py), 126.3 (Ar), 124.1 (CN), 118.5 (Ar), 112.9 (Ar), 107.2 (Py), 16.9 (CH_3); UV-Vis (EtOH) (λ_{max}/nm (log ε)): 429.5 (4.06).

3-cyano-5-phenylazo-6-hydroxy-4-methyl-2--pyridone (**10**). Orange powder; yield: 41%; m.p. 280.6–281.9 °C (lit. m.p. 288.1 °C [28], 278–279 °C [25,26], 278–280 °C [29], 285–286 °C [27]); M = 254.2 g mol^{-1}; FT-IR (KBr, v/cm^{-1}): 3447 (NH hydrazone form), 3149 (NH pyridone), 2229 (CN), 1688, 1647 (C=O pyridone); ^{1}H NMR (200 MHz, DMSO-d_6, δ/ppm): 2.51 (3H, s, CH_3), 7.29 (1H, t, *J* = 7.2 Hz, Ar–H), 7.48 (2H, t, *J* = 7.5 Hz, Ar–H), 7.66 (2H, d, *J* = 7.2 Hz, Ar–H), 12.04 (1H, s, NH pyridone), 14.55 (1H, s, NH hydrazone form); ^{13}C NMR (50 MHz, DMSO-d_6, δ/ppm): 160.4 (Py), 159.7 (Py), 158.4 (Py), 140.6 (Ar), 129.3 (Ar), 126.7 (Ar), 122.6 (Py), 116.8 (Ar), 114.5 (CN), 97.8 (Py), 16.9 (CH_3); UV-Vis (EtOH) (λ_{max}/nm (log ε)): 431.0 (4.72).

3. RESULTS AND DISCUSSION

3.1. Spectral analysis

Based on the FT-IR data, it can be concluded that the investigated pyridone dyes adopt hydrazone form in the solid state. The spectra of the compounds have pronounced peaks originating from carbonyl groups in the ranges 1629–1650 cm^{-1} and 1669–1692 cm^{-1}. The broad spectral bands originating from the –NH vibrations of the hydrazone form are located in the range 3433–3447 cm^{-1}, while the bands originating from the –NH ofpyridone are located in the range 3089–3157 cm^{-1}. ^{1}H NMR and ^{13}C NMR spectra of these compounds were recorded in DMSO-d_6 (**1**–**3**, **10**) and CF_3COOD (**4**, **5**, **7**–**9**) and unambiguously indicate the dominance of hydrazone form in these solvents. It should be noted that spectra of compound **6** were not recorded due to poor solubility in available NMR solvents. ^{1}H NMR chemical shifts assigned to the –N–H proton of the hydrazone form are in the ranges 14.44–14.91 ppm in DMSO-d_6 and 14.87–15.29 ppm in CF_3COOD. Furthermore, the presence of two carbonyl signals in ^{13}C NMR (range 159.7–161.7 ppm in DMSO-d_6 and 163.9–162.4 ppm in CF_3COOD) additionally confirms the presence of hydrazone form. The results obtained by NMR spectral analysis are in accordance with literature data [20,21,29,31]. The great stability and high planarity of the hydrazone form is considered to be mainly influenced by the formation of cooperative intramolecular hydrogen bond of –NH hydrazone and carbonyl group [20,21].

UV-Vis absorption spectra of the mentioned series of compounds in ethanol show an intense peak in the region between 415.5–457 nm (Fig. 4a), which is attributed to the π–π* transition of the hydrazone tautomer [20,21]. The absorption maxima are highly dependent on the position and the electronic nature of the substituents wherein the largest bathochromic shift ($\Delta\lambda_{max}$ = 26 nm) with respect to unsubstituted dye (**10,** 431 nm) is observed for the 4-methoxy substituted dye (**1**), while the largest hypsochromic shift ($\Delta\lambda_{max}$ = 15.5 nm) is observed for 3-nitro substituted dye (**5**).

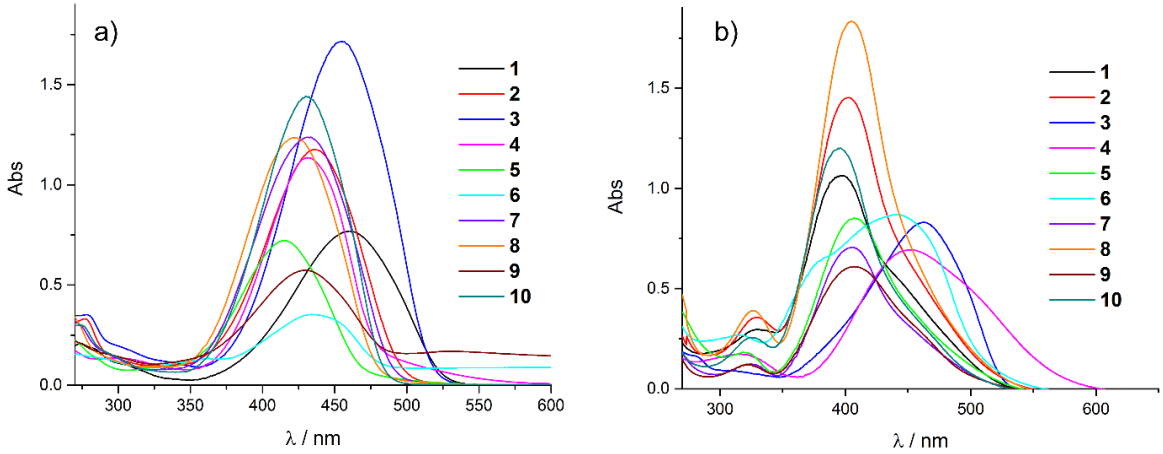

Figure 4. UV-Vis spectra of the synthesized compounds in ethanol (a) and formamide (b)

3.2. Solvatochromic properties of compounds and LSER analysis

The solvatochromic behavior of the investigated dyes was examined in 21 solvents of different dipolarity/polarizability and hydrogen bond capabilities covering a wide range of properties. The UV-Vis spectra in these solvents indicate that the most dominant form in all solvents is hydrazone form [32-34], whereas in amide solvents (DMF, formamide and *N*,*N*-dimethyl acetamide (DMA)) UV-Vis spectra reveal the coexistence of two forms in solution, as evidenced by the appearance of a shoulder in the spectra of all investigated compounds (Fig. 4b). Literature reports on structurally related pyridone azo dyes indicate that azo-hydrazone tautomerism does not occur in these solvents [21,32], instead, deprotonation of

the hydrazone form takes place, leading to an equilibrium between the hydrazone and its anionic form, as illustrated in Fig. 5. Furthermore, in formamide, as well as in DMF and DMA, all spectra exhibit absorption bands in the 300–340 nm range, consistent with the presence of the anionic form in amide solvents [21]. The absorption maxima of hydrazones form in selected solvents are given in Table 1.

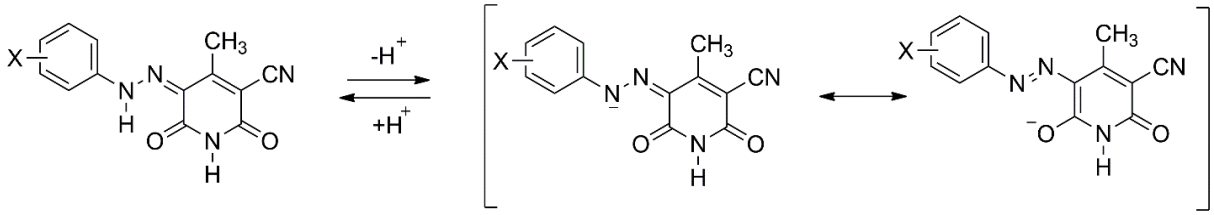

Figure 5. Equilibrium between hydrazone and anionic form in amide solvents.

*Table 1. Absorption maximaof the hydrazone form of compounds (**1–10**) in different solvents.*

	λ_{max} (nm)									
Solvent	**1**	**2**	**3**	**4**	**5**	**6**	**7**	**8**	**9**	**10**
Ethylene glycol	464	440.4	460	429.5	414	437	432	424	430	428.5
Methanol	456.8	435.6	453.5	432	415.5	434	434	424	429.5	431
Ethanol	457	435.6	453	432	415.5	433.5	433.5	423.5	429.5	431
1-Propanol	455	433	455.5	433	414	435.5	431.5	422	431.5	432.5
2-Propanol	456.4	434	443	423	408.5	425	426	419	424.5	423.5
1-Butanol	455.8	435.4	454	434	416.5	434	434.5	425	430.5	432.5
1-Pentanol	460	438.4	450	426	410.5	427	426.5	418	424.5	425
Acetonitrile	456.8	433.4	452	430.5	416.5	436.5	431	425	428.5	429
DMSO	461.2	439.2	459	443.5	424	444	435	427.5	433	432
DMF	458	436.5	453.5	437	422.5	441.5	433	426	430	429
DMA	455	432.5	450.5	431.5	420	439.5	430	424	426	428
Acetone	456.3	432.6	451.5	430.5	415.5	434.5	430.5	423	426.5	428.5
Chloroform	467.4	443	462	434.5	423	440	440.5	433	438	436
Ethyl acetate	453.6	431	449.5	428	414	432	429	421	426.5	427
Methyl acetate	455.2	431.6	449	428	416	432	428.5	422	427	427.5
Tetrahydrofuran	455.8	435	451	431	416	434	430.5	424	427.5	430
Acetic acid	462.5	441	460	434.5	421.5	438	438.5	430	433.5	435.5
Diisopropyl ether	452	431	446	425	413.5	428	430.5	420.5	429	426.5
Dioxane	453.4	433.2	449.5	436	418	435	433	426	427.5	429.5
Pyridine	462	441.5	458	442	425.5	445.5	438.5	432.5	435.5	436.5
Formamide	467.5	444	464	441.5	426.5	450.5	441	433	438	438

According to literature data, the electron density in these dyes is suggested to transfer from the hydrazone bridge to the cyano group, acting as the primary electron acceptor, as well as to the carbonyl group at position 6 of the pyridone ring [20,35]. Corresponding resonance structures are depicted in Fig. 6. It can be observed that the electron rich sites are cyano and carbonyl groups which may serve as suitable donor centers for adsorption onto metal surface. The electron-

donating and electron-withdrawing nature of substituents as well as their position on the phenyl ring significantly influence the electronic distribution of these dyes, thereby affecting electron availability on oxygen and nitrogen atoms of carbonyl and cyano groups, respectively.

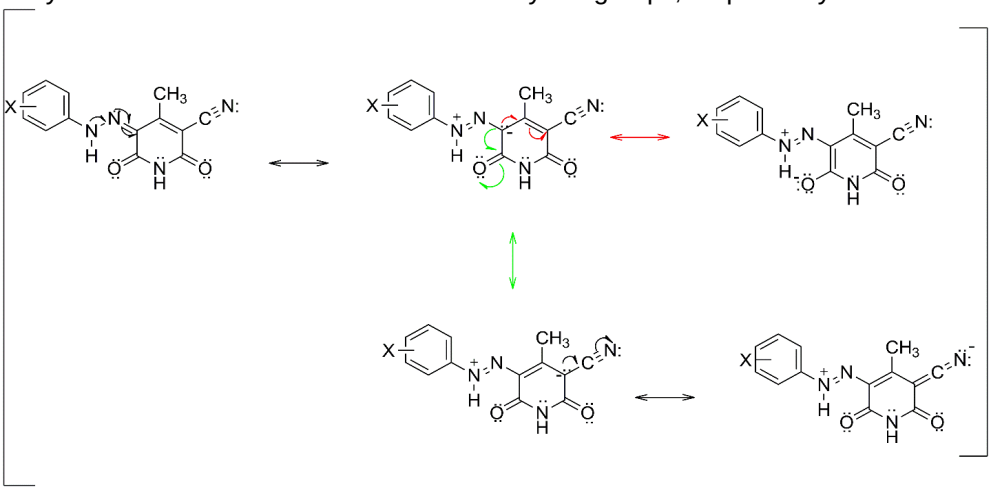

Figure 6. Possible resonance structures of the investigated dyes

The largest bathochromic shift in all solvents is observed for methoxy-substituted dyes (**1**–**3**) when compared to unsubstituted dye (**10**) (Table 1). Electron-donating group such as methoxy stabilize the structure by enhancing intramolecular charge transfer (ICT), thereby increasing electron density at the cyano and carbonyl groups. The UV-Vis absorption maxima of the meta-substituted dyes (**2**, **5**, and **8**) exhibit hypsochromic shift compared to their corresponding *para*- and *ortho*-substituted analogs, as only the inductive effect is operative in the *meta*-position, while resonance stabilization is not feasible. Absorption maxima of *ortho*-substituted dyes (**3**, **7** and **9**) are slightly shifted to lower wavelengths with respect to the corresponding *para*-substituted dyes which can be attributed to steric hindrance that prevents the pyridone and phenyl rings from adopting a planar conformation, thereby reducing effective π-electron delocalization. Electron-accepting nitro groups in the *ortho*- (**6**) and *para*-positions (**4**) are expected to cause a hypsochromic shift, likely due to structural destabilization arising from the development of positive charge on the nitrogen atom, but, in fact,exerts a small bathochromic or negligible (either bathochromic or hypsochromic) shifts which may be due to the counteracting effect of this group to the extended delocalization. Chlorine substituted dye in the *para*-position (**7**), despite strong electron-withdrawing inductive effect, induce a bathochromic shift in the UV-Vis absorption maxima due to their weak resonance effect.

Among the studied solvents, the largest bathochromic shift is observed in highly polar formamide, while shortest wavelengths are found in diisoporpyl ether, 2-propanol and 1-pentanol. According to Table 1, the UV-Vis spectra of the dyes are more affected by changes in the nature and position of the substituents than by alteration in solvent nature.

As shown in Table 1, the solvent effects on the absorption maxima are complex and cannot be attributed to a particular type of solvent interaction. Thus, in order to quantitatively describe manifold solvent-solute interactions LSER models developed by Kamlet-Taft and Catalán are used.Applied to UV-Vis absorption frequencies ν_{max} of hydrazone form of dyes (**1**–**10**) Kamlet-Taft model [36] is given as follows:

$$\nu_{max} = \nu_0 + a\alpha + b\beta + s\pi^* \qquad (1)$$

Each parameter represents a specific type of interaction contributing to the overall solvation ability. The Kamlet-Taft π^* parameter indicates the solvent's dipolarity/polarizability, while α and β correspond to the hydrogen bond donor (HBD) and hydrogen bond acceptor (HBA) capacities, respectively, with their values listed in Table 2. The solvent-independent correlation coefficients *a*, *b*, and *s* quantify the individual contributions of solvent effects on the UV-Vis absorption shifts (ν_{max}). The coefficient ν_0 represents the absorption frequency of the solute in the reference system. The results of regression analysis using the Kamlet-Taft model for compounds **1**–**10**are given in Table 3, while the percentages of solvatochromic parameters for these compounds are given in Table 4. The correlation coefficients (*R*) are above 0.93 indicating high validity of the applied model.

Table 2. Kamlet-Taft [37] and Catalán [38] solvent parameters

No	Solvent	Kamlet-Taft			Catalán			
		*π**	*β*	*α*	*SP*	*SdP*	*SB*	*SA*
1	Ethylene glycol	0.92	0.52	0.9	0.777	0.91	0.534	0.717
2	Methanol	0.6	0.66	0.98	0.608	0.904	0.545	0.605
3	Ethanol	0.54	0.75	0.86	0.633	0.783	0.658	0.4
4	1-Propanol	0.52	0.90	0.84	0.658	0.748	0.782	0.367
5	2-Propanol	0.48	0.84	0.76	0.633	0.808	0.83	0.283
6	1-Butanol	0.47	0.84	0.84	0.674	0.655	0.809	0.341
7	1-Pentanol	0.4	0.86	0.84	0.687	0.587	0.86	0.319
8	Acetonitrile	0.75	0.40	0.19	0.645	0.974	0.286	0.044
9	DMSO	1	0.76	0	0.83	1	0.647	0.072
10	DMF	0.88	0.69	0	0.759	0.977	0.613	0.031
11	DMA	0.88	0.76	0	0.763	0.987	0.65	0.028
12	Acetone	0.71	0.43	0.08	0.651	0.907	0.475	0
13	Chloroform	0.58	0.10	0.20	0.783	0.614	0.071	0.047
14	Ethyl acetate	0.55	0.45	0	0.656	0.603	0.542	0
15	Methyl acetate	0.6	0.42	0	0.645	0.637	0.527	0
16	Tetrahydrofuran	0.58	0.55	0	0.714	0.634	0.591	0
17	Acetic acid	0.64	0.45	1.12	0.651	0.676	0.39	0.689
18	Diisopropyl ether	0.27	0.49	0	0.625	0.324	0.657	0
19	Dioxane	0.55	0.37	0	0.737	0.312	0.444	0
20	Pyridine	0.87	0.64	0	0.842	0.761	0.581	0.033
21	Formamide	0.97	0.48	0.71	0.814	1.006	0.414	0.549

*Table 3. Results of the regression analysis obtained by the Kamlet-Taft equation (**1-10**)*

No	$v_0 \cdot 10^{-3}$ (cm^{-1})	$s \cdot 10^{-3}$ (cm^{-1})	$b \cdot 10^{-3}$ (cm^{-1})	$a \cdot 10^{-3}$ (cm^{-1})	R^a	sd^c	F^b	n^d
1	22.427 (±0.101)	–0.899 (±0.101)	0.222 (±0.110)	–0.250 (±0.042)	0.956	0.066	36	14
2	23.289 (±0.117)	–0.685 (±0.104)	0.262 (±0.131)	–0.188 (±0.053)	0.933	0.080	20	13
3	22.478 (±0.114)	–0.739 (±0.112)	0.408 (±0.153)	–0.360 (±0.051)	0.951	0.082	34	15
4	23.570 (±0.143)	–0.969 (±0.173)	0.605 (±0.154)	–0.254 (±0.076)	0.930	0.108	19	13
5	24.478 (±0.108)	–1.385 (±0.131)	0.701 (±0.107)	–0.136 (±0.058)	0.966	0.085	51	15
6	23.839 (±0.143)	–1.841 (±0.174)	0.639 (±0.146)	–0.168 (±0.076)	0.956	0.115	43	16
7	23.630 (±0.143)	–0.999 (±0.137)	0.549 (±0.140)	–0.382 (±0.059)	0.945	0.085	28	14
8	23.883 (±0.122)	–0.979 (±0.127)	0.678 (±0.129)	–0.240 (±0.056)	0.947	0.082	29	14
9	23.836 (±0.107)	–1.002 (±0.113)	0.394 (±0.117)	–0.270 (±0.048)	0.957	0.070	33	13
10	23.459 (±0.101)	–0.822 (±0.125)	0.788 (±0.103)	–0.295 (±0.055)	0.950	0.080	31	14

[a]Correlation coefficient, [b] Standard deviation, [c]Fisher's test,
[d]Number of solvents included in the correlation.

Based on the values of the independent coefficients (Table 3), it can be concluded that the positions of the UV-Vis absorption maxima depend much more on the change in polarity/polarizability (non-specific interactions) of the solvent than on the change in the HBA and HBD abilities of the solvent. Regression analysis showed that the independent coefficients *s* and *a* are always negative indicating a bathochromic shift by increasing the polarity/polarizability and ability of the solvent todonate hydrogen bonds. Based on this, it can be concluded that the excited state is more stabilized compared to the ground state, as a consequence of solvation. By comparing the absolute values of coefficient *s* (Table 3), it can be observed that this coefficient increases with increasing of electron-withdrawing capability of the substituents, being highest for nitro-substituted dyes. Potential interaction sites between the dye molecules and protic solvents include the cyano and carbonyl groups in the pyridone ring, as well as the nitrogen atom of the hydrazone moiety. Interaction of the hydrogen atom from the protic solvent with the pyridone carbonyl and cyano groups reduces the electron density on oxygen and nitrogen atoms, thereby reinforcing ICT [39] and resulting in a bathochromic shift of the UV-Vis absorption maxima. Conversely, when HBD solvents interact with the lone pair on the N–H group of the hydrazone, the ICT is disrupted, leading to a hypsochromic shift. Overall, the predominant effect is a bathochromic shift with increasing solvent acidity, suggesting that the interaction of HBD solvents is more pronounced with the pyridone ring than with other regions of the molecule.

The positive value of the coefficient *b* for all compounds indicates a hypsochromic shift by increasing the HBD ability of the solvent. The possible interaction sites of the molecule with protophilic solvents are both –NH groups, hydrazone and at the pyridone ring. Considering first interaction, solvent molecules compete with the intramolecular N–H···O hydrogen bond for the hydrogen atom, thereby weakening and elongating the N–H bond and increasing its acidity [40]. As the basicity of the solvent increases, this weakening becomes more pronounced, enhancing electron donation from the –NH group and promoting π-electron delocalization. This enhanced delocalization would lead to a bathochromic shift in the UV–Vis absorption maxima, but in fact in the real system the shift is hypsochromic which could suggest that the interactions with –NH pyridone group are dominant and more intense.

*Table 4. Percentages of solvatochromic parameters determined using the Kamlet-Taft equation (**1–10**).*

Compound	Pπ* (%)	Pβ (%)	Pα (%)
1	65.6	16.2	18.2
2	60.4	23.0	16.6
3	49.1	27.1	23.9
4	53.0	33.1	13.9
5	62.3	31.6	6.1
6	69.5	24.1	6.4
7	51.8	28.4	19.8
8	51.6	35.7	12.7
9	60.1	23.7	16.2
10	43.2	41.3	15.5

Based on Table 4, it is evident that non-specific interactions contribute the most significantly, particularly in the case of nitro-substituted compounds (**4**–**6**). The percentage of dipolarity/ /polarizability of the unsubstituted dye (**10**) is reduced in comparison to the substituted dyes (Table 4), indicating that the substituents on the phenyl core of these compounds intensify non-specific interactions between the dye molecule and the solvent. Additionally, as indicated by Table 4, these dyes show greater sensitivity to the HBA ability of solvents rather than their HBDproperties.

While the Kamlet-Taft approach is quite successful in quantitatively interpreting solvation effects, it does have certain limitations. First, the π* empirical scale combines both solvent dipolarity and polarizability, rather than treating them separately. Second, the empirical solvent parameter scales are derived from the averaged experimental data of multiple solvatochromic probes, which may introduce some generalizations. For this reason, Catalán's four-parameter model was usedfor a more precise analysis [38].

$$\nu_{max} = \nu_0 + aSA + bSB + cSP + dSdP \qquad (2)$$

The advantage of this approach lies in the separation of general interactions into distinct polarizability (*SP*) and dipolarity (*SdP*) components, while scales SA and SB correspond to Kamlet-Taft's *α* and *β* scales (Table 2). Regression analysis according to Eq. 2 is given in Table 5, while percentage contributions of individual parameters are given in Table 6. Thecorrelation coefficient (*R*) of the tested compounds is greater than 0.94.

*Table 5. Results of regression analysis obtained by Catalán's equation (**1–10**).*

No	$v_0 \cdot 10^{-3}$ (cm^{-1})	$c \cdot 10^{-3}$ (cm^{-1})	$d \cdot 10^{-3}$ (cm^{-1})	$b \cdot 10^{-3}$ (cm^{-1})	$a \cdot 10^{-3}$ (cm^{-1})	R^a	sd^c	F^b	n^d
1	22.996 (±0.172)	–1.481 (±0.227)	–0.244 (±0.088)	0.271 (±0.113)	–0.374 (±0.065)	0.953	0.068	32	18
2	24.340 (±0.202)	–2.359 (±0.280)	0.253 (±0.110)	0.292 (±0.101)	–0.617 (±0.085)	0.948	0.079	29	18
3	23.356 (±0.200)	–1.939 (±0.268)	–0.209 (±0.100)	0.557 (±0.115)	–0.465 (±0.077)	0.963	0.079	38	17
4	25.638 (±0.290)	–3.600 (±0.426)	–0.275 (±0.132)	0.421 (±0.193)	–0.437 (±0.127)	0.952	0.100	24	15
5	25.907 (±0.172)	–2.803 (±0.231)	–0.153 (±0. 083)	0.228 (±0.096)	–0.184 (±0.086)	0.973	0.065	52	17
6	25.166 (±0.269)	–3.478 (±0.371)	–0.338 (±0.129)	0.895 (±0.167)	–0.297 (±0.113)	0.964	0.104	42	18
7	24.200 (±0.223)	–2.240 (±0.309)	0.353 (±0.125)	0.537 (±0.114)	–0.626 (±0.093)	0.946	0.086	27	18
8	24.951 (±0.202)	–2.609 (±0.286)	0.245 (±0.115)	0.534 (±0.104)	–0.486 (±0.080)	0.970	0.069	47	17
9	24.362 (±0.215)	–2.304 (±0.298)	0.412 (±0.121)	0.499 (±0.114)	–0.508 (±0.091)	0.947	0.083	26	17
10	24.281 (±0.195)	–1.904 (±0.275)	0.250 (±0.110)	0.317 (±0.112)	–0.576 (±0.083)	0.944	0.075	23	16

[a]Correlation coefficient, [b]Standard deviation,

[c]Fisher's test, [d]Number of solvents included in the correlation

Considering the correlation coefficients (*R*) and number of solvents (*n*), the results of the regression analysis with this model are better than in the case of analysis with the Kamlet-Taft model. Based on Tables 5 and 6, it can be concluded that the most significant influence of the solvent on the absorption maxima of the examined compounds is its polarizability, while dipolarity has a very small influence.

Table 6. Percentages of solvatochromic parameters determined by Catalán's equation (1–10).

Compound	P_{SP} (%)	P_{SdP}(%)	P_B(%)	P_A(%)
1	62.5	10.3	11.4	15.8
2	67.0	7.2	8.3	17.5
3	61.2	6.6	17.6	14.7
4	76.1	5.8	8.9	9.2
5	83.2	4.5	6.8	5.5
6	69.4	6.7	17.9	5.9
7	59.6	9.4	14.3	16.7
8	67.3	6.3	13.8	12.5
9	61.9	11.1	13.4	13.6
10	62.5	8.2	10.4	18.9

As solvent polarizability increases, the π-system distribution is more affected, leading to a bathochromic shift, which is reflected by the negative *c* coefficient for all compounds. The independent *d* coefficient varies depending on the substituent patterns.The polarizability of the solvent have the most profound impact on the solvato chromic behavior of nitro-substituted compounds expressed as the highest values of *c.*

The signs of the coefficients obtained by the Kamlet-Taft and Catalán models are in good agreement. According to the Catalán model, non-specific interactions account for a larger portion of the solvatochromism of these dyes, while solvent basicity accounts for a smaller portion, in contrast to the correlation results produced by the Kamlet-Taft model.The differences between the results from these two models arise from the use of distinct solvatochromic probes to derive the parameters, which consequently reflect different solvent-solute interactions.In contrast, Catalán's empirical solvent scales are based on a well-defined reference system [38], offering a clearer understanding of the interactions between dye and solvent molecules.

In both cases, excellent linear dependences of the calculated wavenumbers on the experimental

values were obtained and are given by the following equations:

The Kamlet-Taft model:

$$v_{calc} = 0.987\ v_{exp} + 0.292\ (R = 0.993,\ n = 141) \quad (3)$$

The Catalán model:

$$v_{calc} = 0.988\ v_{exp} + 0.263\ (R = 0.994,\ n = 171) \quad (4)$$

3.3. Structural aspects for the potential application of synthesized azo dyes as corrosion inhibitors

The ability of a particular organic compound to inhibit metal corrosion is influenced by two factors: the electronic distribution and the chemical structure [11]. Therefore, accurate determination of its structure is essential, as it serves as a fundamental prerequisite for understanding and optimizing its inhibitory performance. Adopting hydrazone form, investigated dyes are multifunctional organic compounds bearing electron-rich sites (Fig. 6), such as carbonyl (–C=O) and cyano (–CN) groups, along with various substituents on the phenyl ring. Substituent nature and position on the phenyl ring significantly affect dye electron distribution, influencing electron availability at oxygen and nitrogen of the carbonyl and cyano groups. Electron-donating groups like methoxy, particularly in *para*- and *ortho*-positions in phenyl ring, enhance ICT, increasing electron density at these sites which in turn could improve their ability to adsorb onto metal surfaces. The structural features of dyes allow them to act as polydentate and chelating ligands when adsorbed onto metal surfaces. Additionally, the presence of the phenyl ring can enhance corrosion inhibition by increasing electron density and improving surface coverage [11,41]. It can be suggested that the hydrazone form favors interaction with metal d-orbitals due to the increased electron density on nitrogen and oxygen atoms. It should also be noted that the increased interaction of free electrons from nitrogen atoms with d-orbitals of metals causes a greater ability to inhibit corrosion. Given these favorable properties, the investigated dyes could be considered a promising corrosion inhibitors for further research studies.

4. CONCLUSION

In this work, the synthesis of ten azo dyes 5--(substituted phenylazo)-3-cyano-6-hydroxy-4--methyl-2-pyridones of different substitution patterns in phenyl ring was carried out. The synthesized dyes adopt hydrazone form in the solid state and deuterated solvents. UV-Vis analysis indicates that solely hydrazone form exists in most of the solvents, while in amide solvents acid-base equilibrium exist. The position of absorption maxima of the hydrazone form is determined by the substitution patterns. UV-Vis spectra of the dyes are more affected by changes in the nature and position of the substituents than by alteration in solvent nature. LSER analysis revealed that the electronic distribution of the synthesized dyes is highly sensitive to the solvent environment, showing increased stabilization in solvents with higher polarizability. Excellent linear dependences of the calculated wavenumbers on the experimental values were obtained in both cases with a slightly better correlation obtained by Catalán model. It should be noted that the hydrazone form of these dyes favors interaction with the d-orbitals of metals due to the increased electron density on the nitrogen and oxygen atoms. Additionally, these compounds serve as a promising starting point for further investigation of their potential to act as corrosion inhibitors. Considering electronic distribution and electronic effect of substituents, dyes bearing electron-donating methoxy groups, particularly in the *ortho*- and para- positions, emerge as most promising candidates for corrosion inhibition.

Acknowledgements

This research has been financially supported by the Ministry of Science, Technological Development and Innovation of the Republic of Serba (Contract No: 451-03-136/2025-03/200287, 451-03-136/2025-03/200135, 451-03-136/2025-03/200178 and 451-03-136/2025-03/200116).

5. REFERENCES

[1] R.I. Alsantali, Q.A. Raja, A.Y.A. Alzahrani, A. Sadiq, N. Naeem, E.U. Mughal, M.M. Al-Rooqi, N.E. Guesmi, Z. Moussa, S.A. Ahmed (2022) Miscellaneous azo dyes: a comprehensive review on recent advancements in biological and industrial applications, Dyes Pigments, 199, 110050. https://doi.org/10.1016/j.dyepig.2021.110050

[2] K. T. Chung (2016) Azo dyes and human health: a review, J. Environ. Sci. Health C, 34(4), 233–261. https://doi.org/10.1080/10590501.2017.1284570.

[3] S. Benkhaya, S. M'rabet, A. El Harf (2020) Classifications, properties, recent synthesis and applications of azo dyes, Heliyon, 6(1), e03271. https://doi.org/10.1016/j.heliyon.2020.e03271

[4] M.S. Kim, B.D. Kwak, G.J. Min, S.H. Park, B.G. Oh, G. Bu, S.H. Cho, J.S. Park, O.Y. Jung (2019), Optical film having good contrast for polarizer and liquid crystal display device. KR Patent, No. *2019078428*.

[5] T. Kawakami, J. Sekiya (2000), Pyridone azo compounds, sublimation-type thermal transfer

pigments, and thermal transfer sheets therefrom. JP Patent, No. *2000239549*.

[6] S. Park, Y. Kang, H. Kwon, H. Kim, S. Kang, H. Lee, C. Yoon, J. Park (2022) Novel Yellow Azo Pyridone Derivatives with Different Halide Atoms for Image-Sensor Color Filters, Molecules, 27(19), 6601. https://doi.org/10.3390/molecules27196601

[7] M. Matsui, R. Aoki, D. Nishiwaki, Y. Kubota, K. Funabiki, J. Jin, T. Yoshida, S. Higashijimad, H. Miura (2015) Importance of fluorescence lifetimes for efficient indoline dyes in dye-sensitized solar cells, RSC Adv., 5, 57721–57724. https://doi.org/10.1039/C5RA09455K

[8] O.M.A. Khamaysa, Selatnia, H. Lgaz, A. Sid, H. Lee, H. Zeghace, M.Benahmed, I.H. Ali, P. Mosset (2021)Hydrazone-based green corrosion inhibitors for API grade carbon steel in HCl: Insights from electrochemical, XPS, and computational studies, Colloid. Surface A, 626, 127047. https://doi.org/10.1016/j.colsurfa.2021.127047

[9] D.S. Chauhan, P. Singh, M. Quraishi (2020) Quinoxaline derivatives as efficient corrosion inhibitors: current status, challenges and future perspectives, J. Mol. Liq., 320, 114387. https://doi.org/10.1016/j.molliq.2020.114387

[10] C. Verma, E.E. Ebenso, M.A. Quraishi, C.M. Hussain (2021) Recent developments in sustainable corrosion inhibitors: design, performance and industrial scale applications, Mat. Adv., 2, 3806-3850. https://doi.org/10.1039/d0ma00681e

[11] N.N. Hau, D.Q. Huong (2023) Effect of aromatic rings on mild steel corrosion inhibition ability of nitrogen heteroatom-containing compounds: Experimental and theoretical investigation, J. Mol. Struct., 1277, 134884. https://doi.org/10.1016/j.molstruc.2022.134884

[12] A.A. Abdulridha, M.A.A.H.Allah, S.Q. Makki, Y. Sert, H.E. Salman, A.A. Balaki(2020) Corrosion inhibition of carbon steel in 1 M H_2SO_4 using new Azo Schiff compound: Electrochemical, gravimetric, adsorption, surface and DFT studies, J. Mol. Liq., 315, 113690 https://doi.org/10.1016/j.molliq.2020.113690

[13] H.M. Elaryian, M.A. Bedair, A.H. Bedair, R.M. Abou shahba, A.E.S. Fouda (2022) Synthesis, characterization of novel coumarin dyes as corrosion inhibitors for mild steel in acidic environment: Experimental, theoretical, and biological studies, J. Mol. Liq., 346, 118310. https://doi.org/10.1016/j.molliq.2021.118310

[14] M.M. Youssif, M.N. El-Nahass, T.A. Fayed, H. A. El-Daly, M.M. El-Gamil, A.M. Eldesoky (2023) Tunable Anticorrosive Effects of Newly Synthesized Benzothiazole Azo Dyes by Potassium Iodide Synergism for Carbon Steel in 1 M HCl: Combined Experimental and Theoretical Studies, ACS Omega, 8(31), 28314-28332. https://doi.org/10.1021/acsomega.3c02105

[15] M. Alfakeer, R.N. Felaly, S.S. AlJuaid, D.F. Seyam, E.M. Mabrouk, M. Abdallah (2025) Synthesis and cyclic voltammetric studies of azo dye compounds derived from 1,5-dihydroxynaphthalene and their application as corrosion inhibitors for carbon steel in hydrochloric acid solution, Int. J. Electrochem. Sc. 20(1), 100892. https://doi.org/10.1016/j.ijoes.2024.100892

[16] K. Shalabi, H.M.A. El-Lateef, M.M. Hammouda, A.A. Abdelhamid (2024) Green Synthesizing and Corrosion Inhibition Characteristics of Azo Compounds on Carbon Steel under Sweet Conditions: Experimental and Theoretical Approaches, ACS Omega, 9(17), 18932–18945. https://doi.org/10.1021/acsomega.3c09072

[17] R. Ganjoo, C. Verma, A.Kumar, M.A. Quraishi (2023) Colloidal and interface aqueous chemistry of dyes: Past, present and future scenarios in corrosion mitigation, Adv. Colloid. Interfac., 311, 102832. https://doi.org/10.1016/j.cis.2022.102832

[18] M.S. Shihab, H.H. Al-Doori (2014) Experimental and theoretical study of [N-substituted] p-amino-azobenzene derivatives as corrosion inhibitors for mild steel in sulfuric acid solution, J. Mol. Struct. 1076, 658–663. https://doi.org/10.1016/j.molstruc.2014.08.038

[19] J. Lađarević, L. Radovanović, B. Božić, A. Mašulović, T. Lunić, Ž. Radovanović, J. Rogan, D. Mijin (2023) New copper (II) complexes derived from azo pyridone dyes: Structure characterization, thermal properties, and molecular docking studies, Appl. Organomet. Chem., 37(10), e7219. https://doi.org/10.1002/aoc.7219

[20] J. Mirković, J. Rogan, D. Poleti, V. Vitnik, Ž.Vitnik, G. Ušćumlić, D. Mijin (2014) On the structures of 5-(4-, 3- and 2-methoxyphenylazo)-3-cyano-1-ethyl-6-hydroxy-4-methyl-2-pyridone: An experimental and theoretical study, Dyes Pigments, 104, 160–168. https://doi.org/10.1016/j.dyepig.2014.01.007

[21] J. Mirković, B. Božić, V. Vitnik, Ž. Vitnik, J. Rogan, D. Poleti, G. Ušćumlić, D. Mijin (2018) Structural, spectroscopic and computational study of 5-(substituted phenylazo)-3-cyano-1-ethyl-6-hydroxy-4-methyl-2-pyridones, Color. Technol., 134(1), 33–43. https://doi.org/10.1111/cote.12321

[22] A. Jezuita, P.A. Wieczorkiewicz, H. Szatylowicz, T.M. Krygowski (2021)Effect of the Solvent and Substituent on Tautomeric Preferences of Amine-Adenine Tautomers, ACS Omega, 6(29),18890–18903. https://doi.org/10.1021/acsomega.1c02118

[23] J.M. Dostanić, D.R. Lončarević, P.T. Branković, Cvetković, D. Jovanović, D.Ž. Mijin (2011) Influence of process parameters on the photodegradation of synthesized azo pyridone dye in TiO2 water suspension under simulated sunlight, J. Environ. Sci. Heal. A, 46(1), 70–79. https://doi.org/10.1080/10934529.2011.526905

[24] J.M. Bobbit, D.A. Scola (1960) Synthesis of Isoquinoline Alkaloids. II. The Synthesis and

Reactions of 4-Methyl-3-pyridinecarboxaldehyde and Other 4-Methyl-3-substituted Pyridines, J. Org. Chem., 25(4), 560–564. https://doi.org/10.1021/jo01074a018

[25] Y.P. Wang, I.J. Wang (1990) Photofading of Azo Pyridone Dyes in Solution: Part II: Substituent Effects on the UV Absorption Spectra and Photostability of 3-(mono- and di-substituted arylazo)-2-hydroxy-4-methyl-5-cyano-6-pyridone in N,N-dimethylformamide, Text. Res. J.,60(9), 519–524.https://doi.org/10.1177/00405175900600090

[26] Y.P. Wang, I.J. Wang (1991) Effects of Substituent and Aggregation on the Photofading of Some Azo Pyridone Dyes on Polyester Substrates, Text. Res. J., 61(3), 162–168. https://doi.org/10.1177/00405175910610030

[27] J. Dostanić, N. Valentić, G. Ušćumlić, D. Mijin (2011) Synthesis of 5-(substituted phenylazo)-6-hydroxy-4-methyl-3- -cyano-2-pyridones from ethyl 3-oxo-2-(substituted phenylazo)butanoates, J. Serb. Chem. Soc.76(4), 499–504. https://doi.org/10.2298/JSC100618044D

[28] C.C. Chen, I.J. Wang (1991) Synthesis of some pyridone azo dyes from 1-substituted 2-hydroxy-6-pyridone derivatives and their colour assessment, Dyes Pigments,15(1), 69–82. https://doi.org/10.1016/0143-7208(91)87008-B

[29] N. Ertan, P. Gurkan (1997) Synthesis and properties of some azo pyridone dyes and their Cu(II) complexes, Dyes Pigments, 33(2), 137–147. https://doi.org/10.1016/S0143-7208(96)00044-7

[30] C.M. Moldovan, O. Oniga, A. Pârvu, B. Tiperciuc, P. Verite, A. Pîrnău, O. Crişan, M. Bojiţă, R. Pop (2011)Synthesis and anti-inflammatory evaluation of some new acyl-hydrazones bearing 2-aryl-thiazole, Eur. J. Med. Chem., 46(2), 526–534. https://doi.org/10.1016/j.ejmech.2010.11.032

[31] A. Alimmari, D. Mijin, R. Vukićević, B. Božić, N. Valentić, V. Vitnik, Ž. Vitnik, G. Ušćumlić (2012) Synthesis, structure and solvatochromic properties of some novel 5-arylazo-6-hydroxy-4-phenyl-3-cyano-2-pyridone dyes, Chem. Cent. J., 6, 71. https://doi.org/10.1186/1752-153X-6-71

[32] A.D. Mašulović, J.M. Lađarević, A.M. Ivanovska, S.Lj Stupar, M.M. Vukčević, M.M. Kostić, D.Ž. Mijin (2021) Structural insight into the fiber dyeing ability: Pyridinium arylazo pyridone dyes, Dyes Pigments, 195, 109741. https://doi.org/10.1016/j.dyepig.2021.109741

[33] B.Đ. Božić, A.S. Alimmari, D.Ž. Mijin, N.V. Valentić, G.S. Ušćumlić (2014) Synthesis, structure and solvatochromic properties of novel dyes derived from 4-(4-nitrophenyl)-3-cyano-2-pyridone, J. Mol. Liq., 196, 61–68. https://doi.org/10.1016/j.molliq.2014.03.026

[34] Q. Peng, M. Li, K. Gao, L. Cheng (1991) Hydrazone-azo tautomerism of pyridone azo dyes: Part II: Relationship between structure and pH values, Dyes Pigments,15(4), 263–274. https://doi.org/10.1016/0143-7208(91)80011-W

[35] J. Lađarević, B. Božić, L. Matović, B. Božić Nedeljković, D. Mijin (2019) Role of the bifurcated intramolecular hydrogen bond on the physicochemical profile of the novel azo pyridone dyes, Dyes Pigments, 162, 562–572, https://doi.org/10.1016/j.dyepig.2018.10.058

[36] M.J. Kamlet, J.M. Abboud, M.H. Abraham, R.W. Taft (1983) Linear Solvation Energy Relationships. 23. A Comprehensive Collection of the Solvatochromic Parameters, π*, α, and β, and Some Methods for Simplifying the Generalized Solvatochromic Equation, J. Org. Chem., 48(17), 2877–2887. https://doi.org/10.1021/jo00165a018.

[37] Y. Marcus (1993)The properties of organic liquids that are relevant to their use as solvating solvents, Chem. Soc. Rev.,22, 409–416. https://doi.org/10.1039/CS9932200409

[38] J. Catalán (2009) Toward a Generalized Treatment of the Solvent Effect Based on Four Empirical Scales: Dipolarity (SdP, a New Scale), Polarizability (SP), Acidity (SA), and Basicity (SB) of the Medium, J. Phys. Chem. B, 113(17), 5951–5960. https://doi.org/10.1021/jp8095727

[39] F.A.S. Chipem, A. Mishra, G. Krishnamoorthy (2012) The role of hydrogen bonding in excited state intramolecular charge transfer. Phys. Chem. Chem. Phys. 14, 8775–8790. https://doi.org/10.1039/C2CP23879A

[40] J. Lađarević, D. Mijin, L. Antonov (2020) Tautomerism in 8-(phenyldiazenyl)quinolin-5-ol: An attempt for pH activated rotary switch, Dyes Pigments, 182, 108628. https://doi.org/10.1016/j.dyepig.2020.108628

[41] P. Wang, Y. Song, Z. Tang, Z. Li, K.R. Ansari, M. Talha, A. Singh, Y. Lin (2024) Systematic Analysis of the Effect of Benzene on the Corrosion Inhibition Performance of Imidazoline Derivatives: Experimental and Theoretical Research,Langmuir, 40(51), 26903 – 26917. https://doi.org/10.1021/acs.langmuir.4c03256

IZVOD

TAUTOMERIJA I SOLVATOHROMIZAM 5-(SUPSTITUISANIH FENILAZO)-3-CIJANO-6-HIDROKSI-4-METIL-2-PIRIDONA

U okviru rada, sintetisano je deset molekula 5-(supstituisanih fenilazo)-3-cijano-6-hidroksi-4-metil-2-piridona, koji se međusobno razlikuju prema položaju i prirodi supstituenata na fenilnom prstenu. Sintetisane boje su detaljno okarakterisane tačkom topljenja i spektroskopskim tehnikama (FT-IR, NMR i UV-Vis). Budući da su elektronska gustina i hemijska struktura organskih molekula od ključne važnosti za njihovu primenu kao inhibitora korozije, ovaj rad se fokusira na određivanje specifičnog tautomernog oblika boja u čvrstom stanju i različitim rastvaračima. Apsorpcioni spektri su određeni u 21 rastvaraču različitih svojstava. Uticaj rastvarača na apsorpcione maksimume određen je LSER metodom (Kamlet-Taft i Catalan modeli). U oba slučaja dobijene su odlične linearne zavisnosti izračunatih talasnih brojeva od eksperimentalnih vrednosti. LSER analiza je pokazala da je solvatohromizam ovih boja prvenstveno određen nespecifičnim interakcijama između molekula boje i rastvarača. Na osnovu analize efekata supstituenata na raspored elektronske gustine ovih boja, boje sa metoksi-grupom u –orto i -para položajima fenilnog jezgra izdvojile su se kao potencijalni kandidati za inhibitore korozije.
***Ključne reči**: piridonske azo boje, tautomerija, hidrazon, LSER*

Naučni rad
Rad primljen: 06.03.2025.
Rad korigovan: 28.05.2025.
Rad prihvaćen: 02.06.2025.

Jelena Lađarević https://orcid.org/ 0000-0002-5554-7295
Bojan Božić https://orcid.org/0000-0001-9910-2741
Dušan Mijin https://orcid.org/0000-0001-5691-2971
Luka Matović https://orcid.org/0000-0003-4945-7776
Nataša Valentić https://orcid.org/0000-0002-5466-7738
Evica Ivanović https://orcid.org/0000-0002-5055-4568
Nebojša Banjac https://orcid.org/0000-0002-4359-6276